Effect of tantalum (Ta) addition and heat treatments on the properties of Ti-rich $Ti_{36}Ni_{49}Zr_{15}$ alloy

Syed Abbas Raza[1,2,3]*(iD), Muhammad Imran Khan[3](iD), Rashid Ali[3](iD),
Muhammad Ramzan Abdul Karim[3](iD)

[1] *Department of Mechanical Engineering, Faculty of Engineering, Gazi University,*
Eti Mah. Yukselis Sk. No. 5, 06570, Maltepe/Ankara, Turkey
[2] *Additive Manufacturing Technologies Research and Application Center-EKTAM, Gazi University, Saray OSB*
Mahallesi, Uzay ve Havacılık OSB Küme Evleri, No. 62, Kahramankazan, Ankara, Turkey
[3] *Faculty of Materials and Chemical Engineering, GIK Institute of Engineering Sciences and Technology,*
Topi-23640, Pakistan

Abstract

$Ti_{36}Ni_{49-x}Zr_{15}Ta_x$ ($x = 5, 10, 15$ at.%) alloys were prepared using a lab-scale arc-melting furnace and homogenized at 1173 K under an argon atmosphere for 2 hours, followed by furnace cooling. The buttons were sliced into 1–2 mm-thick sheets using wire cutting. These sheets were solution-treated under an argon atmosphere, followed by aging and annealing. The results revealed an increase in hardness with Ta addition, due to solid-solution strengthening. With aging and annealing, the hardness decreased due to the softening effect of Ta diffusing from the matrix to form beta phase (β), whose peaks were observed in XRD for the quaternary samples, as well as the development of B2 peaks for the 10 Ta and 15 Ta samples in the diffractogram. Microstructure analysis showed grain refinement with 5 Ta addition. At higher Ta content of 10 and 15 at.%, the martensite structure coarsened due to decreased grain boundary mobility.

1. Introduction

Titanium-nickel (TiNi) shape memory alloys (SMAs) have been widely explored for their unique shape memory and superelastic characteristics [1, 2]. This has led to current and potential research and development across multiple application domains, including automotive, industrial, aerospace, and biomedical sectors [3–6]. This is made possible by extensive research aligned towards understanding the full scope of their properties [7–9]. Research has confirmed that stoichiometric and Ti-rich compositions of TiNi alloys undergo a single-step transformation from a B19' monoclinic low-temperature phase to a B2 austenitic phase, whereas Ni-rich compositions undergo a two-step transformation cycle from Austenite (B2) $\rightarrow$ Orthorhombic (B19) $\rightarrow$ Monoclinic (B19') phase [10–12].

In addition, the Ni-rich system compensates for the mechanical properties by forming fine Ti_3Ni_4 precipitates, thereby optimizing cyclic mechanical and superelastic behavior [13, 14]. In contrast, the Ti-rich alloys contain micron-sized Ti_2Ni-type precipitates that do not provide strengthening due to their incoherency with the matrix [15, 16]. Moreover, a key issue with this binary TiNi system is its low transformation temperature, which limits its scope of use to below 70 °C [17–22]. Certain ternary alloying elements effectively compensate for this and increase the martensite transformation temperature for use, i.e., Pt, Pd, Au, Hf, and Zr. This has led to the exploration and development of high-temperature shape memory alloys [23, 24].

The TiNiZr shape memory alloy system has been touted for requiring lower additions to raise the transformation temperature above 373 K than other op-

---

*Corresponding author: tel.: +905438557309; e-mail addresses: sabbas.raza@gazi.edu.tr , aaraza981@gmail.com

tions, such as TiNiPd, and for being more readily available and cheaper than gold and platinum additions [25]. However, this system faces specific issues that hinder its practical applications. TiNiZr alloy undergoes phase degradation around 1198 K, in which the matrix decomposes into a liquid phase, which is detrimental to the overall system performance. In addition, it exhibits poor cyclic transformation stability, with the transformation temperature decreasing sharply with repeated cycling. Furthermore, Zr addition rapidly deteriorates the workability of the alloy beyond 10 at.%, becoming almost negligible at 25 at.% [26, 27].

To address these issues, quaternary additions have been explored for decades to overcome the limitations of ternary SMAs. In particular, the use of β-phase stabilizer elements such as niobium (Nb) and tantalum (Ta) has been effective in resolving phase and mechanical stability issues and imparting superior chemical resistance [28–34]. This alloy system has been researched previously. Hsieh has conducted in-depth research on the addition of Zr to the properties of TiNi SMA, focusing on the effect of Zr content on transformation temperature, texture, hardness, and the influence of cold rolling on these properties [35]. In a subsequent study, Hsieh evaluated the influence of Zr content on lattice parameters and phase formation [36]. Furthermore, another work reported on a Ti-rich TiNiZr alloy, providing an in-depth evaluation of the microstructural phases and highlighting an incipient melting phase that is detrimental to mechanical properties and forms around 930 ℃ [37]. Zhang worked on Ni-rich materials, evaluating their properties as a function of repeated cold-rolling and heat treatment [38]. However, the influence of the composition of these elements on TiNiZr-based systems has not been thoroughly investigated. The present work investigates the influence of Ta addition on the properties of these arc-melted alloys, as well as the effect of subsequent heat treatment on mechanical properties, microstructure, and phase development. The work will emphasize the use of an atomic force microscope for martensite structure analysis, an optical microscope, XRD to analyze the phases present, and Vickers hardness testing.

2. Experiment

Ti$_{36}$Ni$_{49}$Zr$_{15}$Ta$_x$ (x = 5, 10, 15) alloys were prepared using high-purity (> 99.9 %) elements. The elements were purchased as solid pieces and cold-rolled into thin strips. These were then cut into fine chips (1–2 mm) and weighed using an analytical balance. The chips were cleaned using a 1 : 10 mixture of HF and HNO$_3$, then with analytical-grade acetone in an ultrasonic cleaner. After that, they melt in a Mini Arc Melter (MAM-1) furnace and cast into small buttons.

All the alloy buttons were remelted at least 5 times to ensure homogenization. The buttons were then vacuum-sealed and homogenized at 1173 K for 2 hours in an argon atmosphere, with the specific temperature and time chosen because they provide the minimum temperature required to solutionize the samples by eliminating most second-phase particles [39, 40]. After homogenization, the buttons were cut into thin, small slices 1-2 mm thick using electric discharge machining (EDM), which were then sealed in titanium foil and solution-treated at 1173 K for 1 hour, followed by quenching in ice water. The solution-treated alloys underwent two further heat treatments, namely aging and annealing. In the aging treatment, the solution-treated alloys were heated to 773 K for 1 hour, followed by quenching in ice water; in the annealing treatment, the alloys were cold-rolled to 10 %, heat-treated at 773 K for 1 hour, and subsequently quenched in ice water. The heat-treated alloys were mounted, ground to 2400 grit, and polished with nano-alumina paste and a pad. Optical microscopic (OM) image analysis was performed using an Olympus optical microscope, in which image capture was conducted using an automated adjustment feature in the software for best image capture, and atomic force microscopy (AFM) was performed using Nano-Flex surf AFM, in which a maximum cross-section of 100 µm × 100 µm was used. For etching, a 2 : 2 : 6 volume ratio of H$_2$O, HF, and HNO$_3$ was used to reveal the microstructure. Hardness testing was carried out using Vickers testing with a 50-gram load, with 10 indents per sample; the average was used. Phase analysis was performed using a Bruker XRD instrument with a step size of 0.02° min^{-1} and an angular range of 20°–80°.

3. Phase change by XRD

The XRD analysis was performed to identify the phases formed in the sample. The phase analysis revealed a peak shift, as shown in Figs. 1–4. Different peaks were analyzed to highlight the phases present. The peaks were identified and compared with the literature [41, 42]. The peaks for 35° and 38° were indexed as (001)$_M$ and (110)$_M$ and denoted with 'M'. The (Ti, Zr)$_2$Ni phase peaks were also identified, which agrees with previously published literature [36, 43–45]. The (Ti, Zr)$_2$Ni peaks were identified at 32, 49, and 68 ℃, corresponding to the (511), (422), and (800) crystallographic planes, respectively. The peak at 63° overlaps with the peak for precipitating and oxide formation. The beta (β)-phase peaks were found in 5, 10, and 15 Ta and found to be consistent with previously published work [33, 46, 47].

The key peaks observed with the ternary alloy system correspond to the B19' monoclinic peak and the presence of (Ti, Zr)$_2$Ni-type second-phase particles.

Fig. 1. The combined XRD analysis of the base alloy after heat treatments.

Fig. 2. The combined XRD analysis of the 5 Ta alloy after heat treatments.

Fig. 3. The combined XRD analysis of the 10 Ta alloy after heat treatments.

Fig. 4. The combined XRD analysis of the 15 Ta alloy after heat treatments.

T a b l e 1. The combined XRD analysis of the alloy samples in solution-treated (ST) conditions

S. No	Alloy label	Grain size (μm)	Roughness, Ra (nm)
1	0 Ta ST	0.757	146.1
2	0 Ta An	0.820	147.2
3	0 Ta Ag	18.5	82.5
4	5 Ta ST	0.473	103.9
5	5 Ta An	0.332	175.1
6	5 Ta Ag	0.565	121.0
7	10 Ta ST	0.757	125.0
8	10 Ta An	0.654	130.5
9	10 Ta Ag	0.704	162.9
10	15 Ta ST	0.147	163.2
11	15 Ta An	1.51	125.0
12	15 Ta Ag	219.0	28.1

The monoclinic phase shows strong peaks at $2\theta = 35°$ and $42°$. Furthermore, multiple peaks correspond to second-phase precipitates present in the matrix. This is attributed to the formation of second-phase precipitates during quenching, despite the formation of a homogeneous matrix. The reason not to choose a higher homogenizing temperature was to prevent the formation of the embrittling delta phase, which destabilizes the transformation behavior and shape memory response when the sample is heated at and above 1198 K. Aging and annealing treatments increase peak intensities, particularly of the $(Ti, Zr)_2Ni$-type precipitates [34]. Beta (β)-phase peaks appear with tantalum (Ta) addition in the matrix. With 5 Ta addition, the lower-index peak at $2\theta = 39°$ was prominent, while at higher Ta additions, the higher-order peaks became prominent at approximately $55°$ and $70°$. The transition to higher planar indices for β-phase peaks highlights a change in the growth region, particularly around the B2 phase.
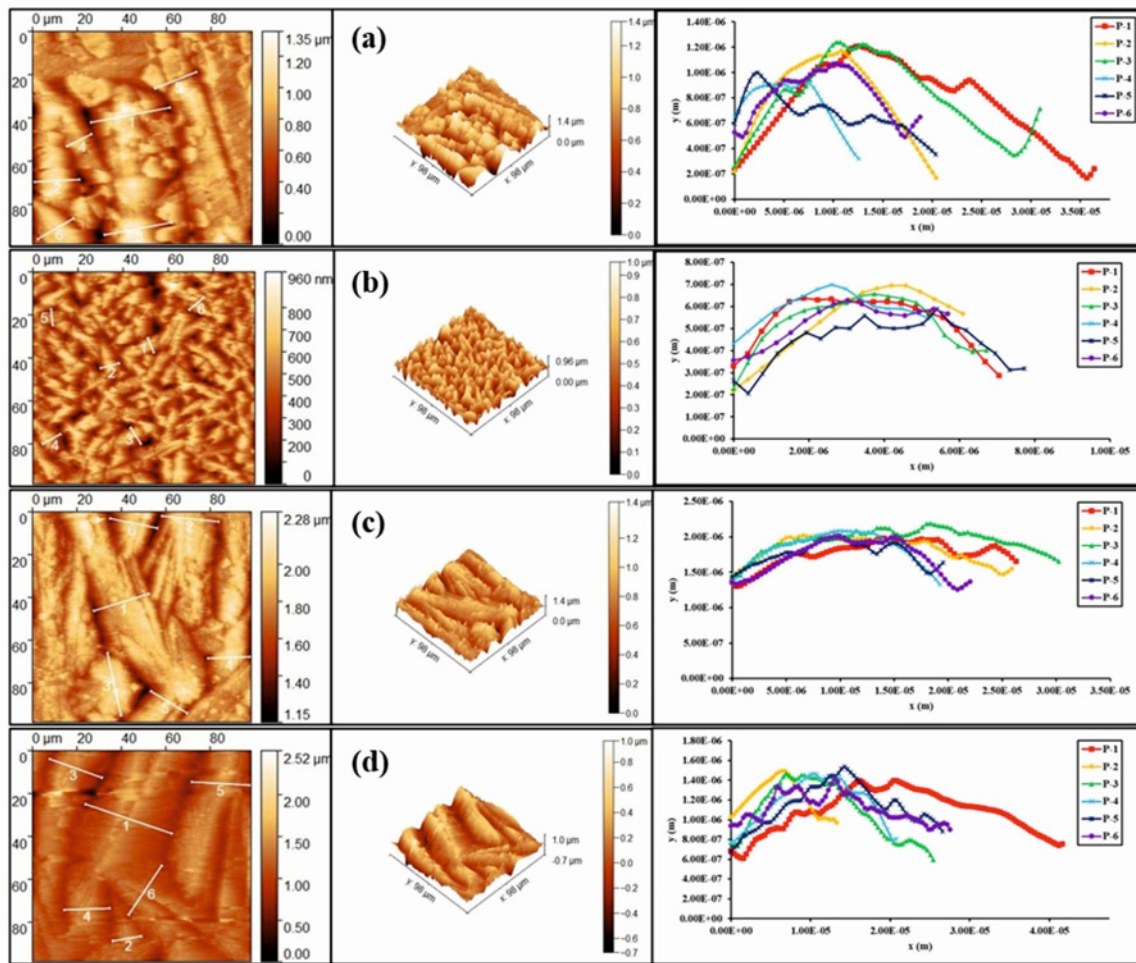
Fig. 5. The combined AFM analysis of the alloy samples in the solution-treated (ST) condition.

Additionally, the aging and annealing treatments benefited the growth of $(Ti, Zr)_2Ni$-type second-phase particles in the matrix, along with the precipitation of the β-phase [48]. The intensity of second-phase precipitates increased primarily in the ternary alloy. With Ta additions of 5, 10, and 15 at.%, the β-phase peaks also showed increased intensity compared to the ST condition, highlighting that aging promoted the diffusion of Ta out of the $(Ti, Zr)(Ni, Ta)$ matrix [49]. The increase in precipitation reduces the ratio of β-forming elements in the matrix and lowers the transformation temperatures, as observed for the base and 5 Ta compositions.

4. Microstructure analysis

The microstructure showed a trend dependent on Ta content; however, it reversed at higher Ta content. This can be either due to a certain solubility limit of Ta in the matrix or the solubility limit varying in the B2 cubic and B19' martensite phase. With 5 % Ta

added, the grain structure was observed to be refined. This is determined quantitatively by calculating the mean martensite variant size using AFM, with values of 0.473, 0.332, and 0.565 nm for 5 Ta in solution-treated, aged, and annealed conditions, respectively. The addition of Ta increased the mean grain size. This is evident in the optical microscope results, which provide a larger observable area. At 5 at.% addition of Ta results in an entirely martensitic matrix [50]. The analysis is shown in Figs. 5–7, and the optical microscope results are highlighted in Figs. 8–10.

The optical microscope results showed that the 10 and 15 Ta samples contained mixed fractions of B19' martensite and a second phase, identified as B2 austenite [51]. The martensite morphology is thin, needle-like when 5 Ta is added to the ternary TiNiZr system, showing an overlapping martensite structure, which transforms to a plate-like morphology with further Ta addition. The 15 Ta optical microscope also reveals the untransformed B2 cubic phase, as evidenced by XRD peaks. The lattice parameters also increase with the increasing Ta content [52, 53]. Furthermore,
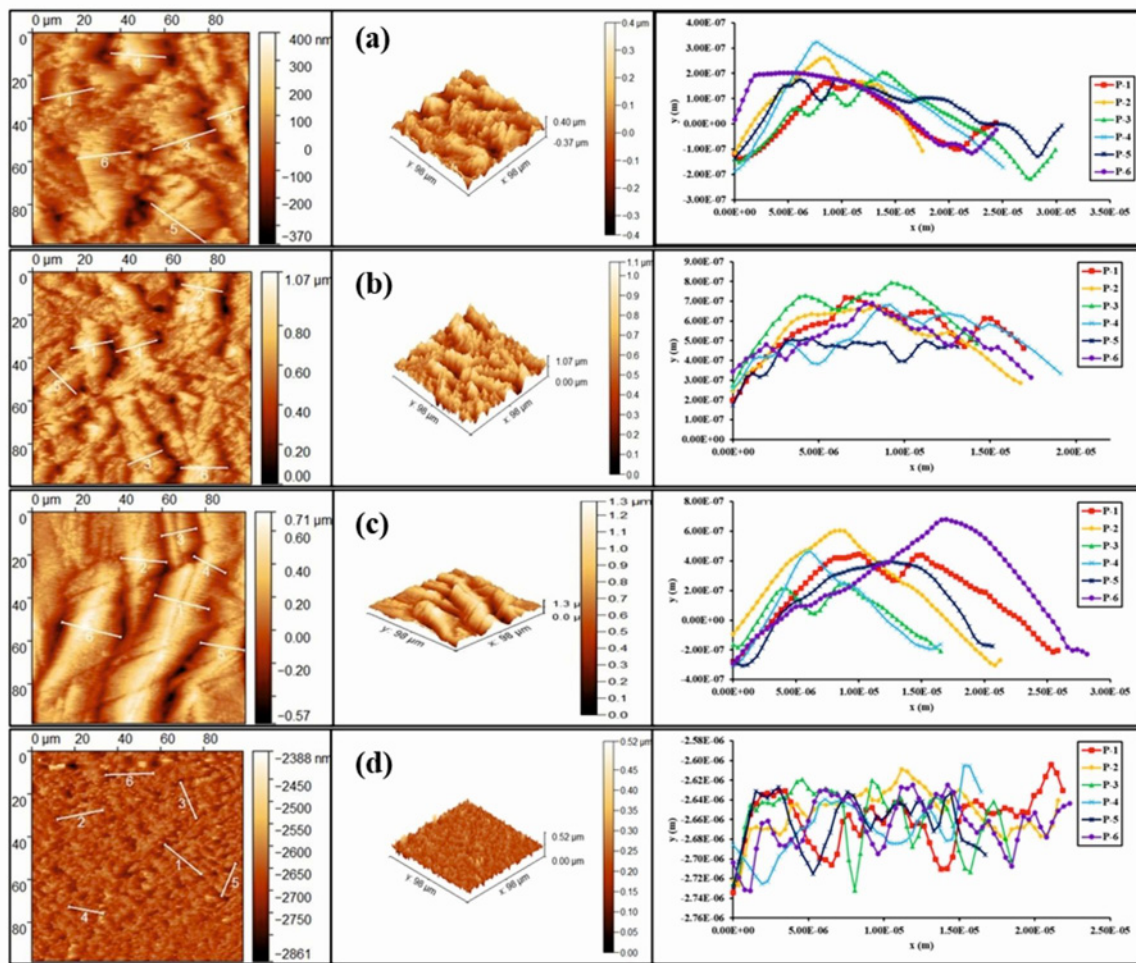
Fig. 6. The combined AFM analysis of the alloy samples in the aged condition.

post-processing treatments alter the morphology of the microstructure. After aging, the base alloy undergoes grain growth, with the mean grain size increasing to 0.565 μm. The annealing treatment further increases the mean martensite size, which is calculated to be 0.332 μm. The increase in martensite could be attributed to a decrease in the enthalpy and entropy of transformation in both the exothermic and endothermic directions when tantalum is added, which reduced the internal friction of transformation [54].

Annealing treatment increases the mean size, though the difference is not significant compared with the ST samples. This indicates that annealing may have provided stress relief in addition to grain growth. More importantly, the dislocations generated by cold rolling increased the lattice strain energy, thereby facilitating grain growth and precipitation in the matrix.

5. Hardness testing

The hardness of the samples is directly correlated

with the volume fraction of Ta and varies with the applied heat treatments, as shown in Fig. 11. As the Ta content increased, the hardness increased due to solid-solution strengthening, which expanded the lattice. This increased to 426.85 from 284.73 for the ternary base composition under the same treatment. Conversely, the hardness of the ST condition is the highest among all three treatments for all the compositions created. The largest observable difference is for 5 Ta, where the ST sample had a hardness of approximately 390 HV, and the aged sample's hardness decreased to 324 HV, the difference being 64 HV.

The annealed sample of the same composition was found to have a slightly higher HV of 335, owing to precipitation into defects and stress-relieving that formed during cold rolling [55].

The hardness also seems to reach saturation as the Ta amount approaches 15 at.%. This indicates that the Ta atoms reach the occupancy limit in the matrix and that second-phase particles provide ineffective strengthening due to their incoherent interface with the matrix. Another key factor to consider is the
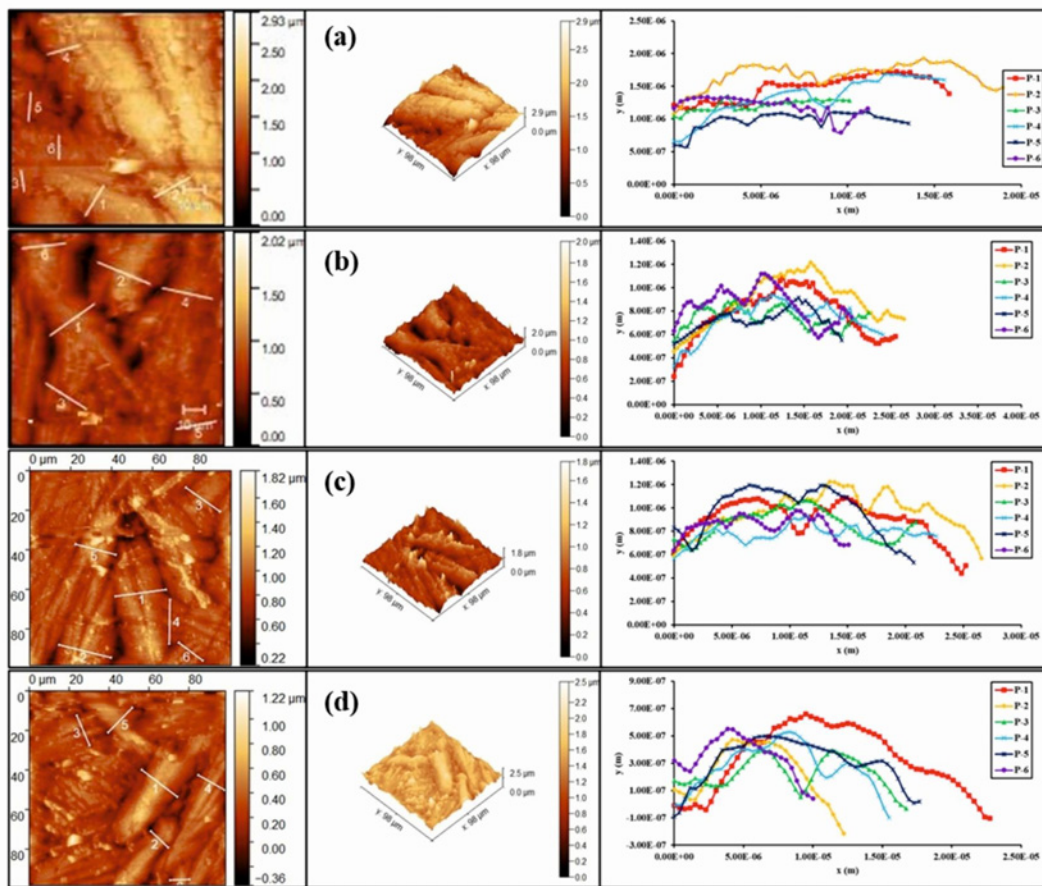
Fig. 7. The combined AFM analysis of the alloy samples in the annealed condition.
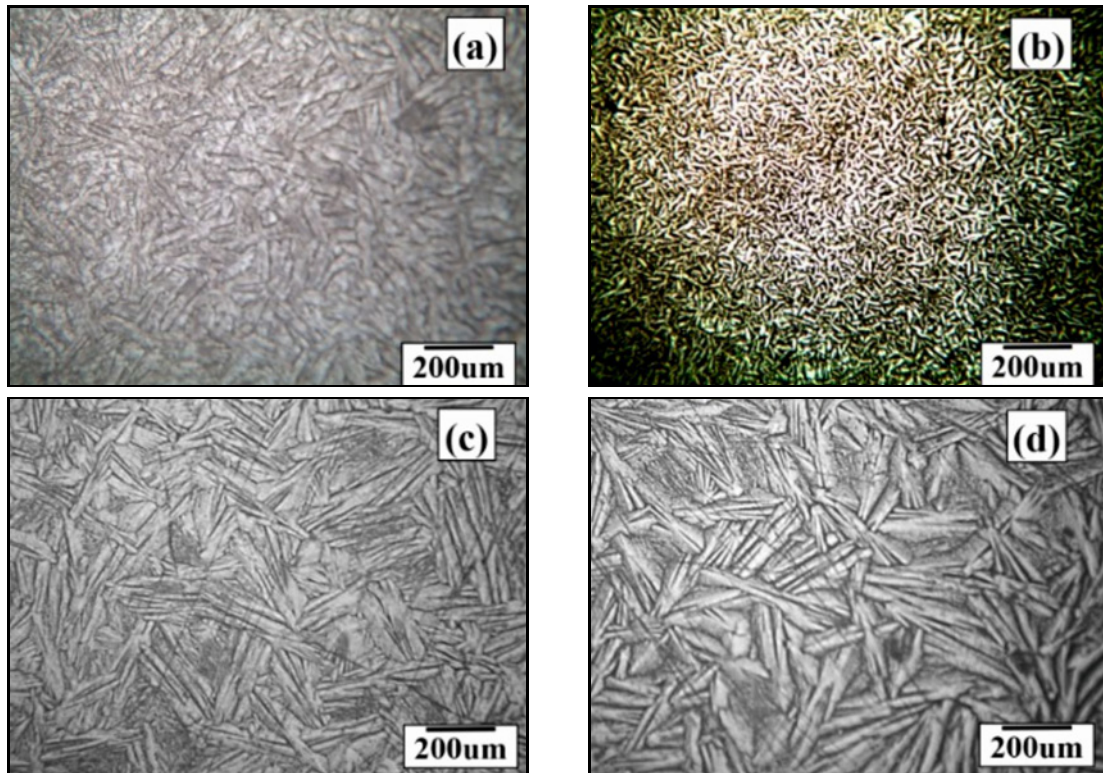

Fig. 8. The optical microscopes of the solution-treated samples are shown in (a) base, (b) 5 Ta, (c) 10 Ta, and (d) 15 Ta.
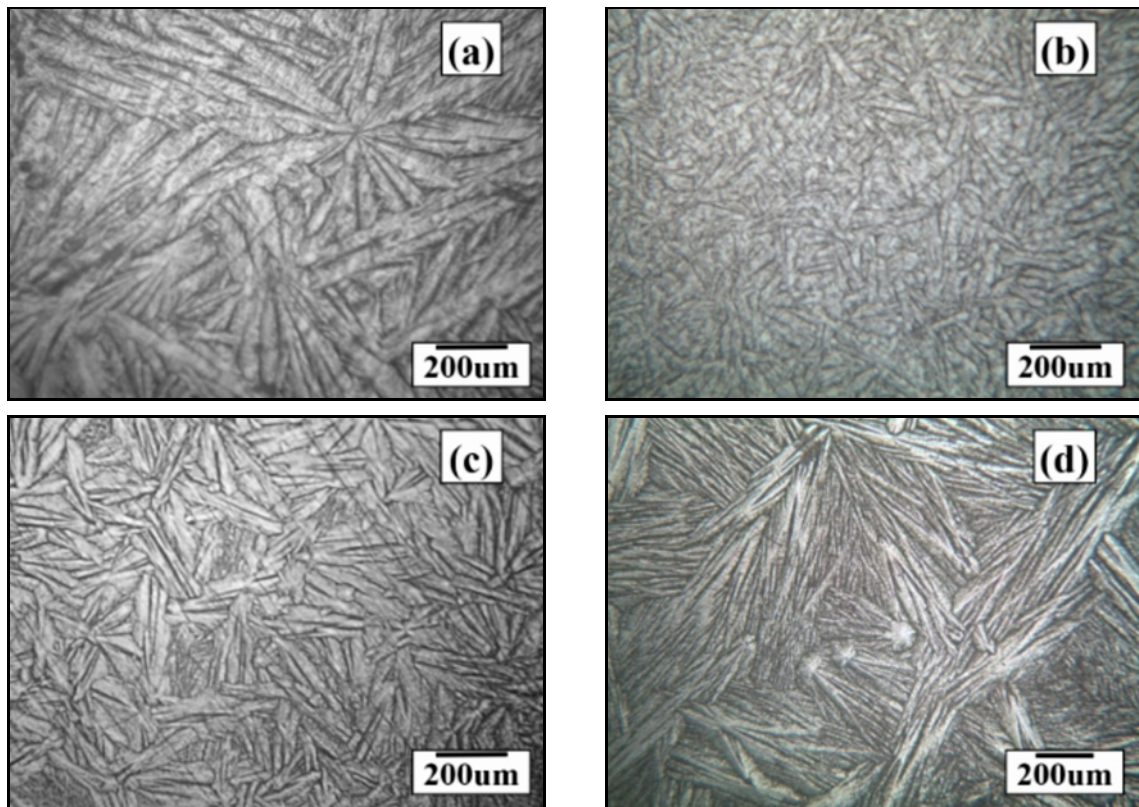
Fig. 9. The optical microscopes of the aged samples are shown in (a) base, (b) 5 Ta, (c) 10 Ta, and (d) 15 Ta.
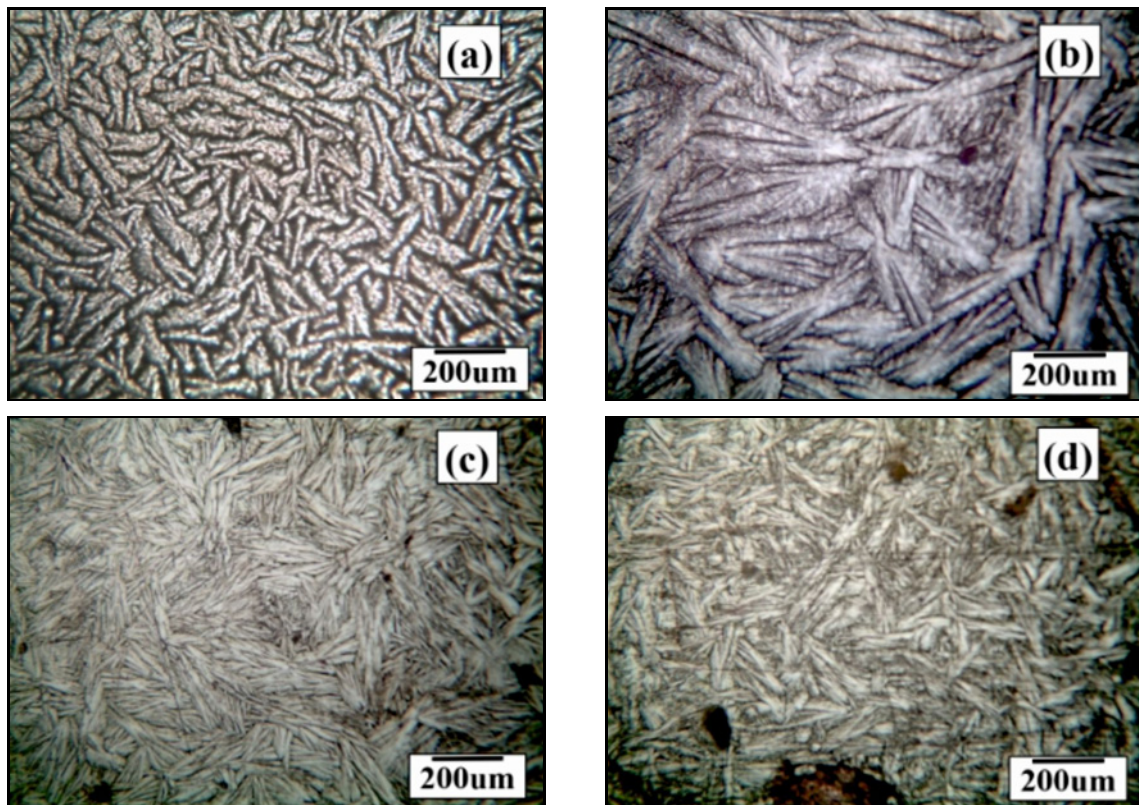

Fig. 10. The optical microscopes of the annealed samples are (a) base, (b) 5 Ta, (c) 10 Ta, and (d) 15 Ta.
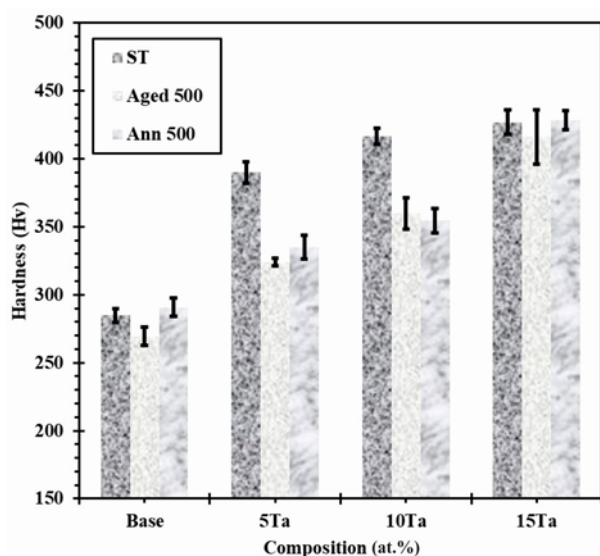
Fig. 11. The hardness values of the alloy samples as a function of different heat treatments.

transformation temperature. With the further addition of the Ta beyond 5 %, the transformation temperature was suppressed below room temperature, and austenite was retained in the matrix. The austenite phase has higher hardness, which could be offset by increased precipitation of the Ta-rich phase in the matrix due to the solubility limit [56]. This is confirmed by the increased intensity of the B2 peaks in the 10 and 15 Ta XRD diffractograms at 2θ values of $41°$ and $45°$, which have superior mechanical properties [57].

The aging treatment exhibited similar behavior, indicating a coherent effect of Ta content on hardness. This also indicates that the trend is unaffected by the retained austenite volume in the matrix. Therefore, the precipitation volume increases with increasing Ta content in the matrix. It may be that a higher Ta content is found in specific regions, though this remains to be studied. Annealing treatment produced a sharper increase in hardness; at 15 Ta, the value was comparable to that of ST samples. This highlights the synergistic effect of cold-rolling and heat treatment on mechanical properties. However, the hardness of the annealed samples does not exceed that of the ST sample, reaching 428 HV, compared with 426 HV for 15 Ta in the ST condition [58].

5. Conclusions

Based on the results analyzed from this study, we have reached the following conclusions:

1. Adding Ta leads to gradual coarsening of martensite structure after refinement at 5 at.% addition.

2. The addition of Ta leads to the formation of increased second precipitates and the Ta-rich β-phase.

3. The heat treatment promotes the precipitation of the second phase $(Ti, Zr)_2Ni$ type phases and Ta-rich β-phase.

4. The addition of Ta also increases the hardness of the alloys. This trend persists in all heat treatments.

References

[1] R. Chaudhari, J. J. Vora, D. M. Parikh, A review on applications of Nitinol shape memory alloy, Lecture Notes in Intelligent Transportation and Infrastructure Part F 1363 (2021) 123–132.
https://doi.org/10.1007/978-981-33-4176-0_10

[2] R. Bogue, Shape-memory materials: A review of technology and applications, Assembly Automation 29 (2009) 214–219.
https://doi.org/10.1108/01445150910972895

[3] L. Stirling, C. H. Yu, J. Miller, E. Hawkes, R. Wood, E. Goldfield, R. Nagpal, Applicability of shape memory alloy wire for an active, soft orthotic, J. Mater. Eng. Perform. 20 (2011) 658–662. https://doi.org/10.1007/S11665-011-9858-7

[4] G. Costanza, M. E. Tata, Shape memory alloys for aerospace, recent developments, and new applications: A short review, Materials 13 (2020) 1856.
https://doi.org/10.3390/MA13081856

[5] M. Balasubramanian, R. Srimath, L. Vignesh, S. Rajesh, Application of shape memory alloys in engineering – A review, J. Phys. Conf. Ser. 2021 (2054) 012078.
https://doi.org/10.1088/1742-6596/2054/1/012078

[6] L. Petrini, F. Migliavacca, Biomedical applications of shape memory alloys, Journal of Metallurgy 2011 (2011) 1–15. https://doi.org/10.1155/2011/501483

[7] A. N. Bucsek, G. A. Hudish, G. S. Bigelow, R. D. Noebe, A. P. Stebner, Composition, compatibility, and the functional performances of ternary NiTiX high-temperature shape memory alloys, Shape Memory and Superelasticity 2 (2016) 62–79.
https://doi.org/10.1007/s40830-016-0052-5

[8] W. J. Buehler, J. V. Gilfrich, R. C. Wiley, Effect of low-temperature phase changes on the mechanical properties of alloys near composition TiNi, J. Appl. Phys. 34 (1963) 1475–1477.
https://doi.org/10.1063/1.1729603

[9] J. Frenzel, A. Wieczorek, I. Opahle, B. Maaß, R. Drautz, G. Eggeler, On the effect of alloy composition on martensite start temperatures and latent heats in Ni–Ti-based shape memory alloys, Acta Mater. 90 (2015) 213–231.
https://doi.org/10.1016/J.ACTAMAT.2015.02.029

[10] J. I. Kim, S. Miyazaki, Effect of nano-scaled precipitates on shape memory behavior of Ti-50.9at.%Ni alloy, Acta Mater. 53 (2005) 4545–4554.
https://doi.org/10.1016/j.actamat.2005.06.009

[11] J. I. Kim, Y. Liu, S. Miyazaki, Ageing-induced two-stage R-phase transformation in Ti-50.9at.%Ni, Acta Mater. 52 (2004) 487–499. https://doi.org/10.1016/j.actamat.2003.09.032

[12] S. Miyazaki, H. Y. Kim, H. Hosoda, Development and characterization of Ni-free Ti-base shape memory and superelastic alloys, Materials Science and Engineering A 438–440 (2006) 18–24. https://doi.org/10.1016/j.msea.2006.02.054

[13] Q. C. Fan, Y. H. Zhang, Y. Y. Wang, M. Y. Sun, Y. T. Meng, S. K. Huang, Y. H. Wen, Influences of transformation behavior and precipitates on the deformation behavior of Ni-rich NiTi alloys, Materials Science and Engineering A 700 (2017) 269–280. https://doi.org/10.1016/j.msea.2017.05.107

[14] J. Michutta, C. Somsen, A. Yawny, A. Dlouhy, G. Eggeler, Elementary martensitic transformation processes in Ni-rich NiTi single crystals with Ni_4Ti_3 precipitates, Acta Mater. 54 (2006) 3525–3542. https://doi.org/10.1016/j.actamat.2006.03.036

[15] X. L. Meng, W. Cai, Y. D. Fu, J. X. Zhang, L. C. Zhao, Martensite structure in Ti-Ni-Hf-Cu quaternary alloy ribbons containing $(Ti,Hf)_2Ni$ precipitates, Acta Mater. 58 (2010) 3751–3763. https://doi.org/10.1016/j.actamat.2010.03.015

[16] L. M. Wu, S. K. Wu, The evolution of Ti_2Ni precipitates in annealed $Ti_{51}Ni_{49}$ shape memory melt-spun ribbons, Philos. Mag. Lett. 90 (2010) 261–268. https://doi.org/10.1080/09500831003630773

[17] J. Khalil-Allafi, A. Dlouhy, G. Eggeler, Ni_4Ti_3-precipitation during aging of NiTi shape memory alloys and its influence on martensitic phase transformations, Acta Mater. 50 (2002) 4255–4274. https://doi.org/10.1016/S1359-6454(02)00257-4

[18] R. J. Wasilewski, S. R. Butler, J. E. Hanlon, On the martensitic transformation in TiNi, Metal Science Journal 1 (1967) 104–110. https://doi.org/10.1179/MSC.1967.1.1.104

[19] J. Khalil-Allafi, G. Eggeler, A. Dlouhy, W. W. Schmahl, C. Somsen, On the influence of heterogeneous precipitation on martensitic transformations in a Ni-rich NiTi shape memory alloy, Materials Science and Engineering A 378 (2004) 148–151. https://doi.org/10.1016/j.msea.2003.10.335

[20] T. H. Nam, T. Saburi, Y. Kawamura, K. Shimizu, Shape memory characteristics associated with the B2 B19 and B19 B19' transformations in a Ti-40Ni-10Cu (at.%) alloy, Materials Transactions, JIM 31 (1990) 262–269. https://doi.org/10.2320/MATERTRANS1989.31.262

[21] H. C. Lin, S. K. Wu, J. C. Lin, The martensitic transformation in Ti-rich TiNi shape memory alloys, Mater. Chem. Phys. 37 (1994) 184–190. https://doi.org/10.1016/0254-0584(94)90091-4

[22] T. Xing, Y. Zheng, L. Cui, Transformation and damping characteristics of NiTi/NiTi alloys synthesized by explosive welding, Mater. Trans. 47 (2006) 658–660. https://doi.org/10.2320/MATERTRANS.47.658

[23] J. Van Humbeeck, Shape memory alloys with high transformation temperatures, Mater. Res. Bull. 47 (2012) 2966–2968. https://doi.org/10.1016/j.materresbull.2012.04.118

[24] J. Ma, I. Karaman, R. D. Noebe, High temperature shape memory alloys, International Materials Reviews 55 (2010) 257–315. https://doi.org/10.1179/095066010X12646898728363

[25] A. P. Ramos, W. B. de Castro, J. D. Costa, R. A. C. de Santana, Influence of zirconium percentage on microhardness and corrosion resistance of $Ti_{50}Ni_{50-x}Zr_x$ shape memory alloys, Materials Research 22 (2019) e20180604. https://doi.org/10.1590/1980-5373-MR-2018-0604

[26] S. F. Hsieh, S. K. Wu, A study on ternary Ti-rich TiNiZr shape memory alloys, Mater. Character. 41(1998) 151–162. https://doi.org/10.1016/S1044-5803(98)00032-1

[27] S. L. Chen, S. F. Hsieh, H. C. Lin, M. H. Lin, J. S. Huang, Electrical discharge machining of TiNiCr and TiNiZr ternary shape memory alloys, Materials Science and Engineering A 445–446 (2007) 486–492. https://doi.org/10.1016/j.msea.2006.09.109

[28] B. Cui, J. Yao, Y. Wu, X. Zhang, F. Wang, J. Sui, W. Cai, Precipitation behavior and mechanical properties of Ti-Ni-Nb-Co alloys, Intermetallics 95 (2018) 40–47. https://doi.org/10.1016/j.intermet.2018.01.014

[29] G. S. Qiu, X. Q. Zhao, L. J. Meng, H. Bin Xu, Effects of Nb on the high temperature mechanical properties of TiNiAl alloys, Mater. Sci. Forum 546–549 (2007) 1477. https://doi.org/10.4028/www.scientific.net/msf.546-549.1477

[30] M. L. Lethabane, P. A. Olubambi, H. K. Chikwanda, Corrosion behaviour of sintered Ti-Ni-Cu-Nb in 0.9 % NaCl environment, Journal of Materials Research and Technology 4 (2015) 367–376. https://doi.org/10.1016/j.jmrt.2015.04.006

[31] G. C. Wang, K. P. Hu, Y. X. Tong, B. Tian, F. Chen, L. Li, Y. F. Zheng, Z. Y. Gao, Influence of Nb content on martensitic transformation and mechanical properties of TiNiCuNb shape memory alloys, Intermetallics 72 (2016) 30–35. https://doi.org/10.1016/j.intermet.2016.01.009

[32] J. Ma, J. Liu, Z. Wang, F. Xue, K. Wu, Z. Pu, Effects of Ta addition on NiTi shape memory alloys, Journal of Materials Science and Technology 16 (2000) 534–536.

[33] S. Cai, J. E. Schaffer, Y. Ren, Effect of Ni/Ti ratio and Ta content on NiTiTa alloys, Shape Memory and Superelasticity 7 (2021) 491–502. https://doi.org/10.1007/s40830-021-00350-1

[34] Z. Lekston, T. Goryczka, Phase transformation in Ti-Ni-Ta shape memory alloy, Solid State Phenomena 130 (2007) 147–150. https://doi.org/10.4028/www.scientific.net/SSP.130.147

[35] S. F. Hsieh, S. K. Wu, A study on ternary Ti-rich TiNiZr shape memory alloys, Materials Characterization 41 (1998) 151–162. https://doi.org/10.1016/S1044-5803(98)00032-1

[36] S. F. Hsieh, S. K. Wu, A study on lattice parameters of martensite in $Ti_{50.5-x}N_{49.5}iZr_x$ shape memory alloys, J. Alloys Compd. 270 (1998) 237–241.

[37] S. F. Hsieh, S. K. Wu, Room-temperature phases observed in $Ti_{53-x}Ni_{47}Zr_x$ high-temperature shape memory alloys, J. Alloys Compd. 266 (1998) 276–282.

[38] J. Zhang, J.-X. Qian, Y.-X. Yang, G.-L. Hao, X.-F. Wang, X.-F. Wang, X.-Y. Li, Q.-P. Xu, Microstructure and mechanical properties of Ni-rich TiNiZr alloy associated with repeated cold-rolling and heat treatment, n.d. https://papers.ssrn.com/sol3/papers.cfm?abstract_id=4625653

[39] S. Gao, O. P. Bodunde, M. Qin, W. H. Liao, P. Guo, Microstructure and phase transformation of nickel-titanium shape memory alloy fabricated by directed energy deposition with in-situ heat treatment, J. Alloys Compd. 898 (2022) 162896.
https://doi.org/10.1016/j.jallcom.2021.162896

[40] K. J. Yuan, Y. Wang, L. J. Zheng, H. Zhang, Microstructural evolution, mechanical properties, and oxidation performance of highly Ni-rich NiTi alloys with added V using vacuum arc melting, J. Alloys Compd. 877 (2021) 160263.
https://doi.org/10.1016/j.jallcom.2021.160263

[41] H. Shahmir, F. Kiani, S. Baradari, N. Resnina, R. Bikbaev, Role of Zr and thermomechanical treatment on phase transformation and functional properties of NiTi-based shape memory alloys, Journal of Materials Research and Technology 26 (2023) 3110–3117.
https://doi.org/10.1016/j.jmrt.2023.08.100

[42] J. K. Lee, W. T. Kim, D. H. Kim, Effects of Pd addition on the glass forming ability and crystallization behavior in the Ni-Zr-Ti alloys, Mater. Lett. 57 (2003) 1514–1519.
https://doi.org/10.1016/S0167-577X(02)01016-9

[43] N. Okada, Y. Fujii, Y. Ishikawa, M. Onoda, H. Y. Kim, S. Miyazaki, Effect of Zr content on shape memory characteristics and workability of Ti-Ni-Zr alloy, J. Japan Inst. Metals 72 (2008) 152–157.
http://dx.doi.org/10.2320/jinstmet.72.152

[44] M. Balcerzak, Electrochemical and structural studies on Ti-Zr-Ni and Ti-Zr-Ni-Pd alloys and composites, J. Alloys Compd. 658 (2016) 576–587.
https://doi.org/10.1016/j.jallcom.2015.10.213

[45] P. Olier, J. C. Brachet, J. L. Bechade, C. Foucher, G. Guénin, Investigation of transformation temperatures, microstructure and shape memory properties of NiTi, NiTiZr and NiTiHf alloys, Journal de Physique IV 05 (1995) C8-741-C8-746.
https://doi.org/10.1051/jp4/199558741

[46] N. M. Lohan, B. Pricop, M. Popa, E. Matcovschi, N. Cimpoeşu, R. Cimpoeşu, B. Istrate, L. G. Bujoreanu, Hot rolling effects on the microstructure and chemical properties of NiTiTa alloys, J. Mater. Eng. Perform. 28 (2019) 7273–7280.
https://doi.org/10.1007/s11665-019-04473-6

[47] K. Inaekyan, V. Brailovski, S. Prokoshkin, V. Pushin, S. Dubinskiy, V. Sheremetyev, Comparative study of structure formation and mechanical behavior of age-hardened Ti-Nb-Zr and Ti-Nb-Ta shape memory alloys, Mater. Charact. 103 (2015) 65–74.
https://doi.org/10.1016/j.matchar.2015.03.016

[48] C. W. Gong, Y. N. Wang, D. Z. Yang, Phase transformation and second phases in ternary Ni-Ti-Ta shape memory alloys, Mater. Chem. Phys. 96 (2006) 183–187.
https://doi.org/10.1016/j.matchemphys.2005.06.057

[49] K. C. Atli, I. Karaman, R. D. Noebe, Influence of tantalum additions on the microstructure and shape memory response of $Ti_{50.5}Ni_{24.5}Pd_{25}$ high-temperature shape memory alloy, Materials Science and Engineering: A 613 (2014) 250–258.
https://doi.org/10.1016/j.msea.2014.06.104

[50] H. Mei, J. C. Liu, F. Chen, Y. X. Tong, M. Zarinejad, Martensitic transformation and shape memory effect of $Ni_{49.6}Ti_{45.4}Ta_5$ shape memory alloy, Mater. Lett. 337 (2023) 133937.
https://doi.org/10.1016/j.matlet.2023.133937

[51] S. Cai, S. G. Mitchell, L. Wang, J. E. Schaffer, Y. Ren, Effect of Ta on microstructures and mechanical properties of NiTi alloys, Shape Memory and Superelasticity 5 (2019) 249–257.
https://doi.org/10.1007/s40830-019-00228-3

[52] S. Cai, J. E. Schaffer, Y. Ren, Effect of Ni/Ti ratio and Ta content on NiTiTa alloys, Shape Memory and Superelasticity 7 (2021) 491–502.
https://doi.org/10.1007/s40830-021-00350-1

[53] J. C. Liu, H. Mei, F. Chen, L. Li, Y. X. Tong, Effect of Ta content on microstructure, martensitic transformation, and shape memory effect of $(Ni_{52.2}Ti_{47.8})_{100-x}Ta_x$ alloys, J. Alloys Compd. 1003 (2024).
https://doi.org/10.1016/j.jallcom.2024.175621

[54] F. Dagdelen, E. Balci, I. N. Qader, Y. Aydogdu, S. Saydam, Effects of substituting Nb with Ta on microstructure and thermal properties of novel biocompatible TiNiNbTa shape memory alloys, Physics of Metals and Metallography 122 (2021) 1572–1580.
https://doi.org/10.1134/S0031918X21140209

[55] A. A. Alhumdany, A. K. Abidali, H. J. Abdulredha, The effect of adding alloying element yttrium and tantalum on mechanical properties of NiTi shape memory alloy, Journal of University of Babylon, Engineering Sciences 26 (2018) 153–164.

[56] E. Balci, F. Dagdelen, Investigation of microhardness and microstructure of Ti-Ni-Nb-X (Ta and V) shape memory alloys, International Journal of Innovative Engineering Applications 5 (2021) 131–135.
https://doi.org/10.46460/ijiea.960655

[57] B. José María Gallardo Fuentes, P. Gümpel, J. Strittmatter, Phase change behavior of nitinol shape memory alloys, Influence of heat and thermomechanical treatments, n.d. 2002.
https://www.osti.gov/etdeweb/biblio/20289309

[58] F. Dagdelen, M. Kok, I. N. Qader, Effects of Ta content on thermodynamic properties and transformation temperatures of shape memory NiTi alloy, Met. Mater. Int. 25 (2019) 1420–1427.
https://doi.org/10.1007/s12540-019-00298-z